Producing Hollow Polymer Microneedles Using Laser Ablated Molds in an Injection Molding Process

Peer-reviewed author version

EVENS, Tim; Van Hileghem, Lorenz; Dal Dosso, Francesco; Lammertyn, Jeroen; Malek, Olivier; Castagne, Sylvie; Seveno, David & VAN BAEL, Albert (2021)
Producing Hollow Polymer Microneedles Using Laser Ablated Molds in an Injection Molding Process. In: JOURNAL OF MICRO AND NANO-MANUFACTURING, 9 (3) (Art N° 030902).

DOI: 10.1115/1.4051456
Handle: http://hdl.handle.net/1942/35958

Producing hollow polymer microneedles using laser ablated molds in an injection molding process

Tim Evens
Department of Materials Engineering Diepenbeek Campus
Wetenschapspark 27, 3590 Diepenbeek, Belgium
tim.evens@kuleuven.be

Lorenz Van Hileghem
KU Leuven, Department of Biosystems – Biosensors Group
Willem de Croylaan 42, box 2428, 3001 Leuven, Belgium
Lorenz.vanhileghem@kuleuven.be

Francesco Dal Dosso
KU Leuven, Department of Biosystems – Biosensors Group
Willem de Croylaan 42, box 2428, 3001 Leuven, Belgium
Francesco.daldosso@kuleuven.be

Jeroen Lammertyn
KU Leuven, Department of Biosystems – Biosensors Group
Willem de Croylaan 42, box 2428, 3001 Leuven, Belgium
Jeroen.lammertyn@kuleuven.be

Olivier Malek
Sirris, Precision Manufacturing
Wetenschapspark 9, 3590 Diepenbeek, Belgium
olivier.malek@sirris.be

Sylvie Castagne
Department of Mechanical Engineering and Flanders Make@KU Leuven-MaPS
Celestijnenlaan 300, 3001 Leuven, Belgium
sylvie.castagne@kuleuven.be

David Seveno
Department of Materials Engineering
Kasteelpark Arenberg 44, 3001 Leuven, Belgium
david.seveno@kuleuven.be

Albert Van Bael
Department of Materials Engineering Diepenbeek Campus
Wetenschapspark 27, 3590 Diepenbeek, Belgium
albert.vanbael@kuleuven.be

ABSTRACT

Microneedle arrays contain needle-like microscopic structures which facilitate drug or vaccine delivery in a minimally invasive way. However, producing hollow microneedles is currently limited by expensive, time consuming and complex microfabrication techniques. In this paper, a novel method to produce hollow polymer microneedles is presented. This method utilizes a femtosecond laser to create hollow microneedle cavities in a mold insert.

This mold insert is used in an injection molding process, to replicate polymethyl methacrylate microneedles. The combined effect of the mold temperature, volumetric injection rate and melt temperature on the replication fidelity was evaluated. It was found that the combination of high injection molding parameters facilitated the replication. Furthermore, the functionality of the manufactured hollow microneedles was successfully tested by injecting a controlled flow of colored water into an agarose matrix. The developed methodology enables the production of low-cost, high-volume microneedle devices, which could be a key asset for large scale vaccination campaigns.

1. INTRODUCTION

Infectious diseases can be tackled both curatively and preventively by the administration of drugs and vaccines, respectively. Although many different administration routes exist, vaccines are most commonly administered by injection [1,2]. Drugs, on the other hand, are more frequently delivered enterally through the oral route, considering its straightforward dosing and wide acceptance [3,4]. Nonetheless, as an effect of passing through the gastrointestinal tract, the bioavailability with enteral

administration can be critically reduced [5]. Therefore, like for vaccines, many drugs are still delivered parenterally by injection to avoid the gastrointestinal tract. Unfortunately, hypodermic needles used in the parenteral delivery approach are known to induce discomfort to the patient, carry the risk of infections and require well-trained medical staff [6,7]. Especially the latter two are known to be problematic in developing countries where about 50% of the needle use is regarded as unsafe [8].

A less invasive parenteral delivery approach is delivery via the skin. This can be done by topically applying formulations or transdermal patches [9]. However, only components with a specific combination of properties can be successfully administered this way, while the large majority of drugs and vaccines are unable to cross the skin's protective barrier, the stratum corneum [10]. Methods to improve absorption rates by surpassing the skin's stratum corneum have been intensively investigated and in 1976, a first concept using microneedles was described in a patent by Alza corporation [4]. Since then, a wide variety of microneedle designs have been developed with needle lengths ranging from 25 to 2500 μm. Usually these designs are developed in arrays which consist of tens or even thousands of individual microneedles [11]. A huge advantage of microneedles is the possibility of pain-free drug delivery and self-administration of drugs and vaccines. An additional advantage for vaccines is the abundance of specialized antigen presenting cells in the skin [4,12]. Moreover, due to their small volume, costs related to distribution are lower compared to traditional hypodermic needles. These benefits offer a great opportunity for delivery of medicines. Further, it is evident that

these systems would worldwide be a significant asset for solving pandemic crises, like the one caused by the COVID-19-virus [13].

In recent work [14], we demonstrated a novel methodology to produce solid polymer microneedles. This method utilizes a femtosecond laser to create cone-shaped micro-cavities in a mold insert. This insert is subsequently used in an injection molding process to create solid cone-shaped microneedles with sharp tip radii. The solid needles can be applied for drug or vaccine delivery using two approaches. In the first approach, referred to as 'poke with patch', the microneedles are used to pierce the skin, creating transient aqueous micro-pores through which a formulation can passively diffuse (Fig. 1a). In the second approach, referred to as 'coat and poke', the needles are coated with a drug or vaccine formulation (Fig. 1b). When inserted in the skin, the coating will be dissolved and the medicine will be deposited in the skin. Although these solid microneedles are able to offer significant advantages compared to the conventional hypodermic needles, their application area is limited because they can only deliver small amounts of medicines [15]. A third type of microneedles are dissolving microneedles. These needles consist of a soluble material, such as a biodegradable polymer, in which the drug or vaccine is encapsulated. A specific approach, referred to as 'poke and release' is used for these microneedles, in which the needles are inserted in the skin, where they dissolve and release the drug or vaccine (Fig. 1c). In contrast to solid and dissolving microneedles, hollow microneedles possess a lumen, or internal bore, which enables the transportation of fluids, thus offering a huge potential (Fig. 1d). This

strategy, referred to as ‘poke and flow’, enables the injection of large amount of drugs [16,17] and vaccines [18] at higher rates.

Undoubtedly, the most challenging problem for hollow microneedles is their complex production process [19]. In fact, a production process to manufacture hollow polymer microneedle arrays in large volumes and at a low cost is currently not available, as it brings an extra level of microfabrication complexity compared to solid microneedles. Current production methods described in literature are mostly very expensive, time consuming or unable to be used as a mass production process. Deep reactive-ion etching has been used to create off-plane hollow microneedles with a lumen of 75 to 150 µm and a length of 700 to 1000 µm [20]. However, the shapes of the microneedles are cylindrical with a blunt tip, which will be difficult to insert into skin. Wang et al. described a two-step production using photolithography and replica molding to produce hollow epoxy microneedles [21]. Inductively coupled plasma and anisotropic wet etching methods were also used to fabricate hollow microneedles on a silicon substrate. These needles were integrated with a piezoelectric pump for insulin dosage [17]. Two studies reported a method to produce hollow glass microneedles by pulling fire-polished glass pipettes [16,22]. The needles were successfully used to deliver insulin to patients with type 1 diabetes in a less painful manner than the conventional hypodermic needles. Stereolithography 3D-printing is another technique suitable to directly create hollow microneedles [23,24] or to create molds [25] which can be used in a replication process to create hollow microneedles. Two-Photon-Polymerization is yet

another additive manufacturing technique which was used in combination with a femtosecond laser to realize the production of hollow microneedles [26].

The choice of fabrication process depends on the selected material, access to manufacturing technology, and the intended application. As a result, a wide variety of needle designs is available in literature. Yet for all of these designs, the shape of the microneedle tip is important, as sharp microneedles are more effective in penetrating the skin. Furthermore, the shape of the microneedle tip is essential for the flow resistance, as a blunt-tipped microneedle will compact the skin and will bear a higher risk of clogging [27,28]. Therefore, microneedles should have a beveled shape, with the lumen off-centered or on the side of the microneedle [12].

In this study, a novel method for producing hollow polymer microneedles using laser ablated molds in an injection molding process is presented. First, two types of hollow microneedle cavities are created through laser ablation and their shape is assessed using micro-computed tomography (μ-CT). Both types of microneedles are implemented on a mold insert, which is afterwards replicated in an injection molding process using three different process conditions. The effect of these conditions on the replication process is assessed by a microscopic study of the obtained microneedles. Eventually, the hollow microneedle design with the highest replication fidelity is further validated during single-needle injections. Hereto, the needle is integrated into a microfluidic chip, which is used to inject colored water into a skin-mimicking agarose matrix.

2. MATERIALS and Methods

2.1. Materials

The thermoplastic material used in this study is polymethyl methacrylate (PMMA) due to its excellent biocompatible nature [29]. The selected grade is Plexiglas 8N from Evonik which has a melt volume flow-rate of 3.00 cm^3/10 min and a glass transition temperature of 117 °C.

The selected mold material is an aluminum zinc alloy (grade 3.4365), which is regularly used for low production series and prototype molds, due to its low cost and good machinability.

Agarose powder and water-based microfluidic dyes were acquired from Melford (UK) and Darwin Microfluidics (France), respectively. Pressure-sensitive adhesive (PSA) tape 200MP 7956MPL from 3M (USA) and transparent PVC sheets of 180 μm thick from Delbo (Belgium) were used for chip fabrication.

2.2. Methods

2.2.1. Representation of the process chain

A micromachining system with a laser source is employed to create hollow microneedle cavities in a mold insert with dimensions 70 mm x 60 mm x 4.6 mm (Fig. 2a). The insert is then placed in the mold (Fig. 2b). Injection molding is used to replicate the micro-cavities (Fig. 2c), creating hollow polymer microneedles on top of a solid flat surface (Fig. 2d). As we want to assess the functionality of the microneedles, a fluidic connection between the needles and the polymer plate is needed. In this study, this connection is created by drilling micro- holes though the flat surface, while in future

work we aim to design a mold to directly incorporate the fluidic connections during injection molding.

2.2.2. Laser machining

A micromachining system (Lasea, Liège, Belgium) with a Satsuma HP femtosecond laser source (Amplitude, San Francisco, USA) is employed to laser ablate a mold insert with dimensions 70 mm x 60 mm x 4.4 mm. The laser source emits a beam with a pulse length of 250 fs, a wavelength of 1030 nm and a pulse repetition rate of 500 kHz. The maximum average power of the laser is 7.85 W, giving a deliverable pulse energy of 15.7 μJ. A galvanometer steers the laser beam within the focal plane, with a spot size of 15.0 μm and a pulse fluence of 8.88 J/cm². Small dust particles which are formed from ablating the metal surface are extracted by a vacuum collect unit. After the laser texturing operation, the mold insert was ultra-sonicated in an ethanol bath for 15 min to remove debris from the micro-holes.

The laser strategy proposed in this work is based on a previous study, in which we developed a method to create cone-shaped micro-holes for the creation of solid microneedles [30]. In this adapted strategy, the laser spot scans a circular region and follows parallel lines in two perpendicular directions, where the distance between two consecutive lines is defined as the hatch pitch. Within the circular region, a scan-free internal area with a specific position is defined to create the lumen of the hollow microneedle. Once the laser has scanned one circular grid, the focal point is lowered with a vertical distance, defined as the layer pitch, and the laser scans again the same area. This process is repeated multiple times for a prescribed number of layers as

illustrated in Fig. 3. Using the proposed strategy, two arrays of 3 x 3 micro-cavities were ablated with different positions of the internal scan-free area. In the first array, the edge of the internal scan-free area is tangential to the edge of the scanned area, while in the second design there is a distance of 100 µm between both edges. In both arrays, the interspacing between the micro-cavities is 1 mm and a 475 µm base diameter was programmed with a hatch pitch of 15 µm. The diameter of the scan-free area is 100 µm and a total of 450 layers was created with an individual layer pitch of 2 µm.

2.2.3. Polymer injection molding

The injection molded part for this study is a 50 mm x 60 mm x 1.5 mm flat plate. The array of micro needles is approximately 2,5 mm x 2,5 mm in size, positioned at a distance of approximately 45 mm from the injection location.

Injection molding was done on an Engel ES 200/35 HL hydraulic injection molding machine (Engel, Schwertberg, Austria) with a maximum clamping force of 350 kN and a 25 mm screw with an L/D ratio of 24.8. The mold temperature is controlled by a WITTMANN TEMPRO Controller (Wittmann, Vienna, Austria). Three sets of injection molding parameters were defined within the recommended limits of the material supplier as given in Table 1. The first set of parameters is defined as ‘low’ and corresponds to the lowest recommended conditions. The second set is defined as ‘middle’ and corresponds to the average between the upper and lower process conditions. The third set is defined as ‘high’ and correspond to the highest recommended conditions. The holding pressure was kept constant in each set of

parameters to completely fill the macroscopic polymer plate without sink marks. In each of the experiments, the parts produced in the first 30 cycles were discarded in order to stabilize the process, then the following parts were collected for characterization.

2.2.3. Micro drilling

The micro drilling tests were carried out on a CNC machining center (Kern Microtechnik, Eschenlohe, Germany) at a spindle speed of 40,000 RPM. A DIXI Polytool 1131 micro drill with a diameter of 100 µm and a length of 700 µm was used. Due to the small length of the micro drill, the thickness of the polymer plate at the location of the microneedles had to be reduced to a thickness of approximately 500 µm. This operation was done using a ProtoTRAK RMX 3500 milling machine (Southwestern Industries, Rancho Dominguez, USA).

2.2.4. Topography characterization

The geometries of the ablated microneedle cavities were characterized using a Phoenix Nanotom µ-CT system (Universal Systems, Solon, USA). The device is equipped with a high-power nanofocus X-ray tube and a diamond-tungsten target was chosen for the high X-ray absorbing aluminum samples. A high-power mode was used to allow focal spot and voxel sizes in the micrometer range. The two arrays of microneedle cavities were cut into cubic samples with an edge length of approximately 3 mm, using a metallographic precision saw. The cubic samples were mounted on a sample holder and fixed on a high-accuracy computer controlled rotation stage. For each scan, 2400 X-ray 2D projection images were obtained from incremental rotation of the scanned samples

over 360°. Acquisition parameters were fixed for all samples as follows: voltage = 100 kV, current = 158 A, voxel size = 3.75 µm, and a 0.1 mm copper filter was used during scanning. Reconstruction of the acquired 2D projections into 3D volumes was performed using GE Phoenix datos|x REC software. Reconstructed datasets (slices) were exported for further analysis and visualization within Fiji ImageJ. Before conducting measurements, the Nanotom instrument was calibrated using a calibration rod (Goekeler Messtechnik, VTX18CE000-022), having an uncertainty of 1.0 µm. For each set of laser parameters, one cubic sample containing nine micro-holes were measured. The average length and diameter of the nine micro-cavities, along with the standard deviation was reported in the results.

The geometry of the replicated thermoplastic microneedles were assessed using a Keyence VH-S30 digital microscope (Keyence, Osaka, Japan) with a maximum magnification of X200. The system was connected to a VHX-500F monitor with built-in measuring software. The microscope was calibrated using a stage micrometer (Olympus Tokyo, OBMM 1/100) which has an uncertainty of 0.5 µm. Ten injection molded samples were collected and on each sample one microneedle was measured. The averages of these ten measurements along with the standard deviations are reported in the results.

2.2.5. Preparation of a skin-mimicking substrate

An agarose gel with concentration of 2.65% (w/v) was prepared by dissolving the agarose powder in distilled water by heating on a hot plate under constant magnetic stirring until the solution had completely cleared out (±20 minutes). Then, the solution was poured into a petri dish to obtain a gel of about 1 cm thick. The substrates were

used for injection experiments at least two hours after solidification and on the same day.

2.2.5. Validation of single-needle injections

Channels of 1 mm width were cut from the PSA using a CO2 laser cutter (Speedy 300, Trotec Laser, Plymouth, USA). With this fabrication method, the channel height is defined by the thickness of the PSA tape, in this case being 153 µm. The PVC layers, designed to contain also the connection holes for the microneedle and pump, were cut with a digital craft cutter (Maxx Air 24 in., KNK, USA). After chip assembly (Fig. 4) by exerting pressure on the well-aligned and sandwiched layers, the microneedle with its substrate was integrated using a laser cut PSA connector piece to assure a tight sealing.

To inject distilled water with a 1/100 diluted blue dye into a (biological) matrix, a fluid flow was controlled by the setup as shown in Figure 5. Using a pressure controller (LineUp^{TM} Push/Pull, Fluigent, France) and a flow sensor (S model, Fluigent, France), injections into the agarose matrix were controlled while monitoring the obtained pressures in real-time every second (1 Hz). To guarantee a good insertion of the microneedles into the agarose slab throughout the experiment, a small weight was applied on top of the chip after manually inserting the microneedle. Injection profiles were followed-up by filming the process from the side using a smartphone camera and snapshots of the recorded dispersion profiles after 0, 2, 5, 10 and 15 minutes were collected. The injection was repeated 3 times on 3 different agarose slabs and the average pressure along with one standard deviation are reported in the results.

3. RESULTS AND DISCUSSION

3.1. Laser ablation

Two arrays of 3 x 3 microneedle cavities were formed during the laser ablation process, which took approximately 9.5 minutes for each array. Cross sectional views of the produced micro-cavities for both arrays are depicted in Figure 6. The XY images represent cross sections throughout the depth of the cavity, while the XZ and YZ images represent cross sections throughout the width of the cavity. The distance below each image indicates the position of the cross section. For XY, 0 μm corresponds to the mold surface, while for XZ and YZ 0 μm corresponds to the edge of the microneedle.

In both arrays, we can observe that the internal scan-free area has formed a tapered feature inside the micro-cavity, which will form the lumen of the hollow microneedle. The position of the tapered feature is different for both arrays due to the difference in position of the internal scan-free area. For array 1, the distance between the edge of the tapered feature and the edge of the micro-hole is only a few micrometers, while for array 2 this distance is approximately 100 μm. Evidently, the laser will also ablate material in the region between the tapered feature and the edge of the micro-hole, therefore inducing a trench between the tapered feature and the edge of the micro-hole. The depth of this trench in array 2 is much deeper compared to the trench in array 1, being 508 ± 11 μm and 110 ± 9 μm, respectively. This discrepancy can be explained by the larger surface area of array 2, which will cause higher accumulated energy in this region compared to array 1.

Cone-shaped micro-holes with an internal tapered feature can be observed for both arrays. The formation of this conical shape is expected to be the result of two laser phenomena, being laser reflectance on steep sidewalls and possibly a plasma shieling effect. First, steep sidewalls will cause most of the laser light to be reflected rather than absorbed. Therefore, the ablation efficiency near the edge of the cavity is drastically reduced, causing the diameter to become smaller as the micro-hole is created [31]. Moreover, the reflected laser light will partially be redirected to the bottom of the hole, contributing to a deeper and sharper cavity. A possible second phenomenon occurs for laser ablation processes with high repetition rates [32]. Vaporized material that is unable to escape from the micro-cavity interacts with the next incoming laser pulse, forming a plasma. This plasma will defocus the laser beam, creating a protective shield referred to as “plasma shielding”.

The cavity diameters at the mold surface are similar for both arrays, being 504 ± 5 µm for array 1 and 510 ± 3 µm for array 2. However, these dimensions are higher than the programmed base diameter of 475 µm. This difference can be explained as follows. During the laser ablation process, the laser focal spot is progressively moved deeper inside the mold material. Therefore, the Gaussian-shaped laser beam will start to intersect with the edge of the already created micro-hole. If in this intersecting region the power density of the Gaussian beam is higher than the ablation threshold, additional material will be removed. Thus, during the laser ablation process, the micro-cavities will progressively increase in diameter. Secondly, the depth of the micro-cavities in array 1 are deeper compared to the cavities in array 2 being 1513 ± 12 µm and

1318 ± 12 µm, respectively. As in array 2, the internal scan-free area is located more towards the center of the micro-hole, less energy can be induced in the center region of the micro-hole, resulting in shallower holes compared to array 1.

We can observe low standard deviations for the cavity depth, cavity diameter at and the depth of the trench. In fact, the highest coefficient of variation for all of the measurements corresponds to approximately 3 %. This indicates a very high repeatability of the laser ablation process.

3.2. Replication through injection molding

Fig. 7 shows an image of the replicated polymer microneedles of array 1 created with a scan-free internal area close to the edge of the needle (Fig 7a), and array 2 created with a scan-free area close to the center of the needle (Fig 7b). These samples were created with the 'high' injection molding parameters at a cycle time of approximately 18 seconds. For both arrays, we observe hollow cone-shaped microneedles with a bevel shaped tip, which is similar to conventional hypodermic needles. The trench which was formed between the tapered feature and the edge of the micro-cavity has now been replicated to form an upstanding ridge which partially encloses the sides of the lumen. This could be beneficial, as the ridge could prevent fluids from leaking between the microneedle and the skin of the patient when the microneedle has not completely penetrated in the skin. In the further stages of this paper we continue using only array 2, as these needles have the highest potential to form functional microneedles.

The three different sets of injection molding parameters were used to replicate the microneedle cavities from array 2. Figure 8 shows the microscopic images of the front and side view of the replicated microneedles and Figure 9 shows the measured needle length, ridge height and tip wall thickness of the replicated microneedles in function of the three different sets of injection molding parameters. In addition, the replication of the microneedle in height was expressed, calculated based on the length of the needle and the depth of the corresponding micro-cavity. It is to be noted that the volumetric replication fidelity will be much higher than the expressed percentage of the replication in height. This due to the fact that the volume gradually decreases throughout the height of the cone-shaped needles.

The three parameters that were varied between the different sets of injection molding parameters are the melt temperature, the volumetric injection rate and the mold temperature. All of these parameters will, to some extent, influence the replication of the microneedles. The first parameter is the mold temperature, which is in literature known to be the most important parameter when it comes to replicating micro-features [33–35]. When a macro-scale cavity with micro-features is injection molded, the filling of the micro-features has to compete with the filling in the rest of the cavity. Since the polymer will follow the path of least resistance, most of the material will flow in the main flow direction through the macro-scale cavity, leaving the micro-features only partially filled, also known as the hesitation effect [36,37]. These micro-features will then only be filled after the rest of the cavity is filled and the pressure rises. Yet, as soon as the polymer is in contact with the mold, a layer of frozen polymer

material (skin layer) will be formed. The rapid solidification of the skin layer hinders the filling of the micro-features and can lead to incomplete filling [38]. By increasing the mold temperature, the formation of the frozen layer can be delayed, leading to the polymer still being able to be deformed during the packing phase, resulting in a better replication of the micro-features [39–41]. The second parameter is the volumetric injection rate. High volumetric injection rates reduce the injection time and can prevent premature freezing of the polymer. Moreover, a high injection velocity promotes shear heating, which can locally decrease the melt viscosity and can therefore improve the replication [33]. The highest volumetric injection rate used in this study was set to the limit of the injection molding equipment. The last parameter is the melt temperature. High temperatures of melt ensure lower melt viscosity, lower cavity pressure drop, and the ability of the melt to flow into micro-features [42]. The upper melt temperature is limited, as it should be selected consistent with the polymer properties to avoid thermal degradation.

It can clearly be observed that there is a significant difference in replication fidelity between the three different injection molding conditions. The low injection molding parameters resulted in the shortest microneedles having a very low ridge and a large wall thickness of the needle tip. The needles created with the ‘middle’ parameters are already better compared to the needles obtained with the low injection molding parameters. Yet, the highest replication fidelity is observed for the ‘high’ injection molding parameters. Here, the tallest needles are found combined with a high ridge and low tip wall thickness. Besides, these microneedles have the lowest standard deviation

for all of the measurements. This indicates a more stable injection molding process, which in turn results in a high reproducibility of the produced samples. Furthermore, the microneedles created with the 'high' injection molding conditions appear to be more opaque compared to the other two sets of microneedles. This opaque appearance is caused by micro- and nano surface roughness, which are replicated using the 'high' process conditions. The replication of the microneedles will also be affected by the volumetric shrinkage of the polymer. This volumetric shrinkage can be determined using the compressibility (or PVT) behavior of the polymer and can be modelled by the double domain Tait equations [43]. An estimate of the volumetric shrinkage can be calculated by assuming the pressure at the end of the packing stage to be equal to the holding pressure and the temperature to be equal to the no-flow temperature. Consequently, a linear shrinkage of 0.28 % was calculated for the PC material, which corresponds to only a very small portion of the incomplete replication.

Not only the tip of the microneedle is subjected to incomplete replication, but also the ridge of the microneedle will be affected. In fact, the ridge of the microneedle is much more sensitive to incomplete replication as the aspect ratio of this component is much higher. With an increase in aspect ratio, the surface area to volume ratio increases, which corresponds to a higher heat transfer between the molten polymer and the mold surface [44]. This results in a faster solidification of the polymer, causing a higher fraction of incomplete filling. For the microneedles replicated with the low injection molding conditions, the filling of in height of the ridge corresponds to only 20 %.

3.3. Validation on skin-mimicking substrate

To proof that the microneedles are compatible with microfluidic technologies for injecting drug or vaccine substances, single microneedles were integrated into a chip connected to a pressure pump. Performing injections with a single microneedle was preferred over arrays to reduce complexity while studying release profiles and phenomena like leakage. The patch was vertically inserted into a 2.65% (w/v) agarose gel to mimic intradermal injection [45,46]. As the gel is transparent, the injection profile could be followed-up easily by the blue colored water.

The frames and graph in Figure 10 show the dispersion profile through the agarose and pressure profile during the injection of 7.5 µL of colored water at a flow rate of 0.5 µL/min, respectively. Pressure data were corrected for the pressure required to maintain the flow through the setup, including the chip with microneedle, without insertion into the skin model. The results clearly depict that after a few minutes a constant pressure is reached and maintained, indicating a constant flow from the microneedle into the matrix. The injected liquid could be observed by the naked eye after approximately one minute, after which a uniform release profile consistently evolved. This proves the feasibility of the microneedles to inject liquids when integrated in a microfluidic platform.

4. Conclusion

In this study, a novel method to produce hollow polymer microneedles was successfully demonstrated. We were able to create hollow microneedle cavities in an aluminum mold insert by laser ablation. The position of the lumen inside the microneedle was changed by adapting the laser scanning strategy. Polymer injection molding was used to replicate the hollow microneedles using three sets of molding conditions. The replication fidelity for each of these conditions was evaluated through microscopic measurements. It was found that the combination of a high mold temperature, volumetric injection rate and melt temperature facilitated the replication. At last, the functionality of the manufactured hollow microneedles was evaluated during single-needle injections. We effectively injected colored water into an agarose matrix using a pressure pump. The developed methodology has a huge potential, as it acts as a mass production technique for low-cost, high-volume microneedle devices. Moreover, it is possible to change the design of the microneedle by adjusting the laser scanning parameters, which allows for further improvements.

In the nearby future, we will attempt to directly incorporate the fluidic connections between the needles and the polymer plate during the injection molding process, by adapting the mold design. Besides, we will further improve the microneedle design in terms of functionality for different conditions and applications.

ACKNOWLEDGMENT

The authors would like to thank Shashwat Kushwaha for his guidance in micro drilling the polymer samples at the KU Leuven NanoCenter.

FUNDING

This work was funded by the KU Leuven Interdisciplinary Network project IDN/20/011 - MIRACLE: Autonomous microfluidic patch for plasmid-based vaccine.

REFERENCES

[1] Hegde NR, Kaveri S V., Bayry J. Recent advances in the administration of vaccines for infectious diseases: Microneedles as painless delivery devices for mass vaccination. Drug Discov Today 2011;16:1061–8. https://doi.org/10.1016/j.drudis.2011.07.004.

[2] Zuckerman JN. The importance of injecting vaccines into muscle. Br Med J 2000;321:1237–8. https://doi.org/10.1136/bmj.321.7271.1237.

[3] Tucak A, Sirbubalo M, Hindija L, Rahić O, Hadžiabdić J, Muhamedagić K, et al. Microneedles: Characteristics, materials, production methods and commercial development. Micromachines 2020;11. https://doi.org/10.3390/mi11110961.

[4] Donnelly RF, Singh TRR, Larrañeta E, McCrudden MTC. Microneedles for Drug and Vaccine Delivery and Patient Monitoring. Chichester: 2018. https://doi.org/10.1002/9781119305101.

[5] Guillot AJ, Cordeiro AS, Donnelly RF, Montesinos MC, Garrigues TM, Melero A. Microneedle-based delivery: An overview of current applications and trends. Pharmaceutics 2020;12:1–28. https://doi.org/10.3390/pharmaceutics12060569.

[6] Mooney K, McElnay JC, Donnelly RF. Children's views on microneedle use as an alternative to blood sampling for patient monitoring. Int J Pharm Pract 2014;22:335–44. https://doi.org/10.1111/ijpp.12081.

[7] Cross S, Roberts M. Physical Enhancement of Transdermal Drug Application: Is Delivery Technology Keeping up with Pharmaceutical Development? Curr Drug Deliv 2005;1:81–92. https://doi.org/10.2174/1567201043480045.

[8] Simonsen L, Kane A, Lloyd J, Zaffran M, Kane M. Unsafe injections in the developing world and transmission of bloodborne pathogens: A review. Bull World Health Organ 1999;77:789–800.

[9] Cheung K, Das DB. Microneedles for drug delivery: trends and progress. Drug Deliv 2016;23:2338–54. https://doi.org/10.3109/10717544.2014.986309.

[10] Paudel KS, Milewski M, Swadley CL, Brogden NK, Ghosh P, Stinchcomb AL. Challenges and opportunities in dermal/transdermal delivery. Ther Deliv 2010;1:109–31. https://doi.org/10.4155/tde.10.16.

[11] Juster H, van der Aar B, de Brouwer H. A review on microfabrication of thermoplastic polymer-based microneedle arrays. Polym Eng Sci 2019;59:877–90.

https://doi.org/10.1002/pen.25078.
[12] Li X (James), Zhou Y. Microfluidic devices for biomedical applications. Woodhead Publ. Ser. Biomater., Cambridge: Woodhead Publishing Limited; 2013, p. 1–652.
[13] Kim E, Erdos G, Huang S, Kenniston TW, Balmert SC, Carey CD, et al. Microneedle array delivered recombinant coronavirus vaccines: Immunogenicity and rapid translational development. EBioMedicine 2020;55:1–12. https://doi.org/10.1016/j.ebiom.2020.102743.
[14] Evens T, Malek O, Castagne S, Seveno D, Van Bael A. A novel method for producing solid polymer microneedles using laser ablated moulds in an injection moulding process. Manuf Lett 2020;24:29–32. https://doi.org/10.1016/j.mfglet.2020.03.009.
[15] Roxhed N, Griss P, Stemme G. Membrane-sealed hollow microneedles and related administration schemes for transdermal drug delivery. Biomed Microdevices 2008;10:271–9. https://doi.org/10.1007/s10544-007-9133-8.
[16] Gupta J, Felner EI, Prausnitz MR. Erratum: Minimally invasive insulin delivery in subjects with type 1 diabetes using hollow microneedles (Diabetes Technology and Therapeutics (2009) 11:6 (329-337)). Diabetes Technol Ther 2009;11:471. https://doi.org/10.1089/dia.2009.0729.
[17] Ma B, Liu S, Gan Z, Liu G, Cai X, Zhang H, et al. A PZT insulin pump integrated with a silicon microneedle array for transdermal drug delivery. Microfluid Nanofluidics 2006;2:417–23. https://doi.org/10.1007/s10404-006-0083-x.
[18] Giri Nandagopal MS, Antony R, Rangabhashiyam S, Sreekumar N, Selvaraju N. Overview of microneedle system: A third generation transdermal drug delivery approach. Microsyst Technol 2014;20:1249–72. https://doi.org/10.1007/s00542-014-2233-5.
[19] Faraji Rad Z, Nordon RE, Anthony CJ, Bilston L, Prewett PD, Arns J-Y, et al. High-fidelity replication of thermoplastic microneedles with open microfluidic channels. Microsystems Nanoeng 2017;3:1–11. https://doi.org/10.1038/micronano.2017.34.
[20] Liu Y, Eng PF, Guy OJ, Roberts K, Ashraf H, Knight N. Advanced deep reactive-ion etching technology for hollow microneedles for transdermal blood sampling and drug delivery. IET Nanobiotechnology 2013;7:59–62. https://doi.org/10.1049/iet-nbt.2012.0018.
[21] Wang PC, Wester BA, Rajaraman S, Paik SJ, Kim SH, Allen MG. Hollow polymer microneedle array fabricated by photolithography process combined with micromolding technique. Proc 31st Annu Int Conf IEEE Eng Med Biol Soc Eng Futur Biomed EMBC 2009 2009:7026–9. https://doi.org/10.1109/IEMBS.2009.5333317.
[22] Martanto W, Moore JS, Kashlan O, Kamath R, Wang PM, O'Neal JM, et al. Microinfusion using hollow microneedles. Pharm Res 2006;23:104–13. https://doi.org/10.1007/s11095-005-8498-8.
[23] Yeung C, Chen S, King B, Lin H, King K, Akhtar F, et al. A 3D-printed microfluidic-enabled hollow microneedle architecture for transdermal drug delivery. Biomicrofluidics 2019;13. https://doi.org/10.1063/1.5127778.
[24] Ceyssens F, Chaudhri BP, Van Hoof C, Puers R. Fabrication process for tall, sharp,

hollow, high aspect ratio polymer microneedles on a platform. J Micromechanics Microengineering 2013;23. https://doi.org/10.1088/0960-1317/23/7/075023.

[25] Krieger KJ, Bertollo N, Dangol M, Sheridan JT, Lowery MM, O'Cearbhaill ED. Simple and customizable method for fabrication of high-aspect ratio microneedle molds using low-cost 3D printing. Microsystems Nanoeng 2019;5. https://doi.org/10.1038/s41378-019-0088-8.

[26] Trautmann A, Roth GL, Nujiqi B, Walther T, Hellmann R. Towards a versatile point-of-care system combining femtosecond laser generated microfluidic channels and direct laser written microneedle arrays. Microsystems Nanoeng 2019;5. https://doi.org/10.1038/s41378-019-0046-5.

[27] Bodhale DW, Nisar A, Afzulpurkar N. Structural and microfluidic analysis of hollow side-open polymeric microneedles for transdermal drug delivery applications. Microfluid Nanofluidics 2010;8:373–92. https://doi.org/10.1007/s10404-009-0467-9.

[28] Luttge R, Berenschot EJW, de Boer MJ, Altpeter DM, Vrouwe EX, van den Berg A, et al. Integrated lithographic molding for microneedle-based devices. J Microelectromechanical Syst 2007;16:872–84. https://doi.org/10.1109/JMEMS.2007.899339.

[29] Frazer RQ, Byron RT, Osborne PB, West KP. PMMA: An essential material in medicine and dentistry. J Long Term Eff Med Implants 2005;15:629–39. https://doi.org/10.1615/JLongTermEffMedImplants.v15.i6.60.

[30] Evens T, Malek O, Castagne S, Seveno D, Bael A Van. Controlling the geometry of laser ablated microneedle cavities in different mould materials and assessing the replication fidelity within polymer injection moulding. J Manuf Process 2021;62:535–45. https://doi.org/10.1016/j.jmapro.2020.12.035.

[31] Audouard E, Mottay E. Engineering model for ultrafast laser microprocessing. Front Ultrafast Opt Biomed Sci Ind Appl XVI 2016;9740:974016. https://doi.org/https://doi.org/10.1088/0022-3727/34/18/327.

[32] Cheng J, Perrie W, Edwardson SP, Fearon E, Dearden G, Watkins KG. Effects of laser operating parameters on metals micromachining with ultrafast lasers. Appl Surf Sci 2009;256:1514–20. https://doi.org/10.1016/j.apsusc.2009.09.013.

[33] Tosello G. Micro Injection Molding. München: Carl Hanser Verlag GmbH & Co. KG; 2018. https://doi.org/10.3139/9781569906545.

[34] Attia UM, Marson S, Alcock JR. Micro-injection moulding of polymer microfluidic devices. Microfluid Nanofluidics 2009;7:1–28. https://doi.org/10.1007/s10404-009-0421-x.

[35] Baruffi F, Gülçür M, Calaon M, Romano JM, Penchev P, Dimov S, et al. Correlating nano-scale surface replication accuracy and cavity temperature in micro-injection moulding using in-line process control and high-speed thermal imaging. J Manuf Process 2019;47:367–81. https://doi.org/10.1016/j.jmapro.2019.08.017.

[36] Yao D, Kim B. Injection molding high aspect ratio microfeatures. J Inject Molding Technol 2002;6:11–7.

[37] Masato D, Sorgato M, Lucchetta G. Characterization of the micro injection-compression molding process for the replication of high aspect ratio micro-

structured surfaces. Microsyst Technol 2017;23:3661–70. https://doi.org/10.1007/s00542-016-3149-z.
[38] Gornik C. Injection moulding of parts with microstructured surfaces for medical applications. Macromol Symp 2004;217:365–74. https://doi.org/10.1002/masy.200451332.
[39] Rytka C, Kristiansen PM, Neyer A. Iso- and variothermal injection compression moulding of polymer micro- and nanostructures for optical and medical applications. J Micromechanics Microengineering 2015;25:1–16. https://doi.org/10.1088/0960-1317/25/6/065008.
[40] Sorgato M, Lucchetta G. The evaluation of vacuum venting and variotherm process for improving the replication by injection molding of high aspect ratio micro features for biomedical application. AIP Conf Proc 2015;1664. https://doi.org/10.1063/1.4918483.
[41] Vera J, Brulez AC, Contraires E, Larochette M, Trannoy-Orban N, Pignon M, et al. Factors influencing microinjection molding replication quality. J Micromechanics Microengineering 2018;28. https://doi.org/10.1088/1361-6439/aa9a4e.
[42] Packianather M, Griffiths C, Kadir W. Micro injection moulding process parameter tuning. Procedia CIRP 2015;33:400–5. https://doi.org/10.1016/j.procir.2015.06.093.
[43] Kazmer DO. Injection Mold Design Engineering. München: Carl Hanser Verlag GmbH & Co. KG; 2007. https://doi.org/10.3139/9783446434196.
[44] Hill SDJ, Kämper KP, Dasbach U, Döpper J, Erhfeld W, Kaupert M. An investigation of computer modelling for micro-injection moulding. Proc Microsym'95 1995;12:275–83.
[45] Zhang D, Das DB, Rielly CD. Microneedle Assisted Micro-Particle Delivery from Gene Guns: Experiments using skin-mimicking agarose gel. J Pharm Sci 2014;103:613–27. https://doi.org/10.1002/jps.23835.
[46] Dal Dosso F, Kokalj T, Belotserkovsky J, Spasic D, Lammertyn J. Self-powered infusion microfluidic pump for ex vivo drug delivery. Biomed Microdevices 2018;20:1–11. https://doi.org/10.1007/s10544-018-0289-1.

Figure Captions List

Fig. 1 A schematic representation of the different types of microneedles. (a) solid microneedles, (b) coated microneedles, (c) dissolving microneedles, and (d) hollow microneedles for drug and vaccine delivery. Base on figure from [19].

Fig. 2 Illustration of the process chain to produce hollow polymer microneedles

Fig. 3 Illustration of the laser strategy with internal scan-free area

Fig. 4 Exploded view of the chip containing a single, straight microfluidic channel. A single microneedle was tightly incorporated into the chip by a PSA connecting piece. At the other end of the channel, a hole serves for connecting a fluidic pump.

Fig. 5 Setup for controlling the injection into agarose. From left to right the pressure controller, a pressurized reservoir containing the to be injected liquid, the flow sensor with feedback to the pressure controller, the microfluidic chip with integrated microneedle and the agarose slab.

Fig. 6 Cross sectional views obtained from the µ-CT measurements of the micro-hole arrays, with the scan-free area: (a) close to the edge of the needle and (b) close to the center of the needle. The distance below each image indicates the position of the cross section. For XY, 0 µm corresponds to the mold surface, while for XZ and YZ 0 µm corresponds to the edge of the microneedle.

Fig. 7 Microscopic image of the replicated polymer microneedle arrays created with a scan-free internal area (a) close to the edge of the needle, and (b) close to the center of the needle.

Fig. 8 Microscopic image of the front and side view of the replicated polymer microneedles created with: (a) ‘low’ injection molding parameters, (b) ‘middle’ injection molding parameters and (c) ‘high’ injection molding parameters. The average value of the dimensions of the needles are reported together with the standard deviation (n = 10).

Fig. 9 (a) Needle length, (b) ridge height and (c) tip wall thickness of the replicated microneedles from array 2 in function of the three different sets of injection molding parameters, being ‘low’, ‘middle’ and ‘high’. The percentages in (a) represent the replication in height.

Fig. 10 Injection profiles accompanied with the pressure obtained during injection through a single microneedle into skin-mimicking agarose at 0.5 µL/min. The black curve shows the average obtained pressure profile (n = 3) and the grey shaded area shows one standard deviation.

Table Caption List

Table 1 Three sets of injection molding parameters: ‘low’, ‘middle’ and ‘high’

Table 1

	Low	Middle	High
Melt temperature [°C]	240	250	260
Volumetric injection rate [cm^3/s]	50	100	150
Holding pressure [Bar]	800	800	800
Mold temperature [°C]	70	90	110

Fig. 1

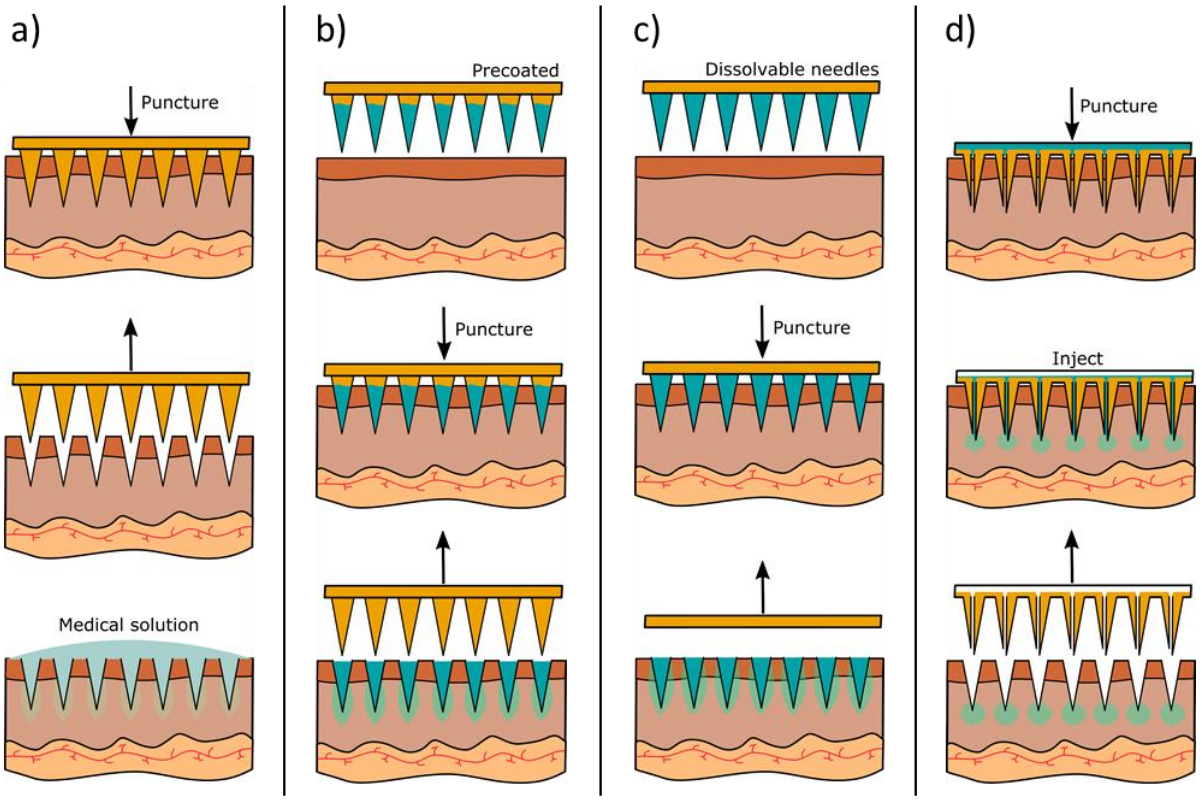
a)
Puncture
Medical solution
b)
Precoated
Puncture
c)
Dissolvable needles
Puncture
d)
Puncture
Inject

Fig. 2

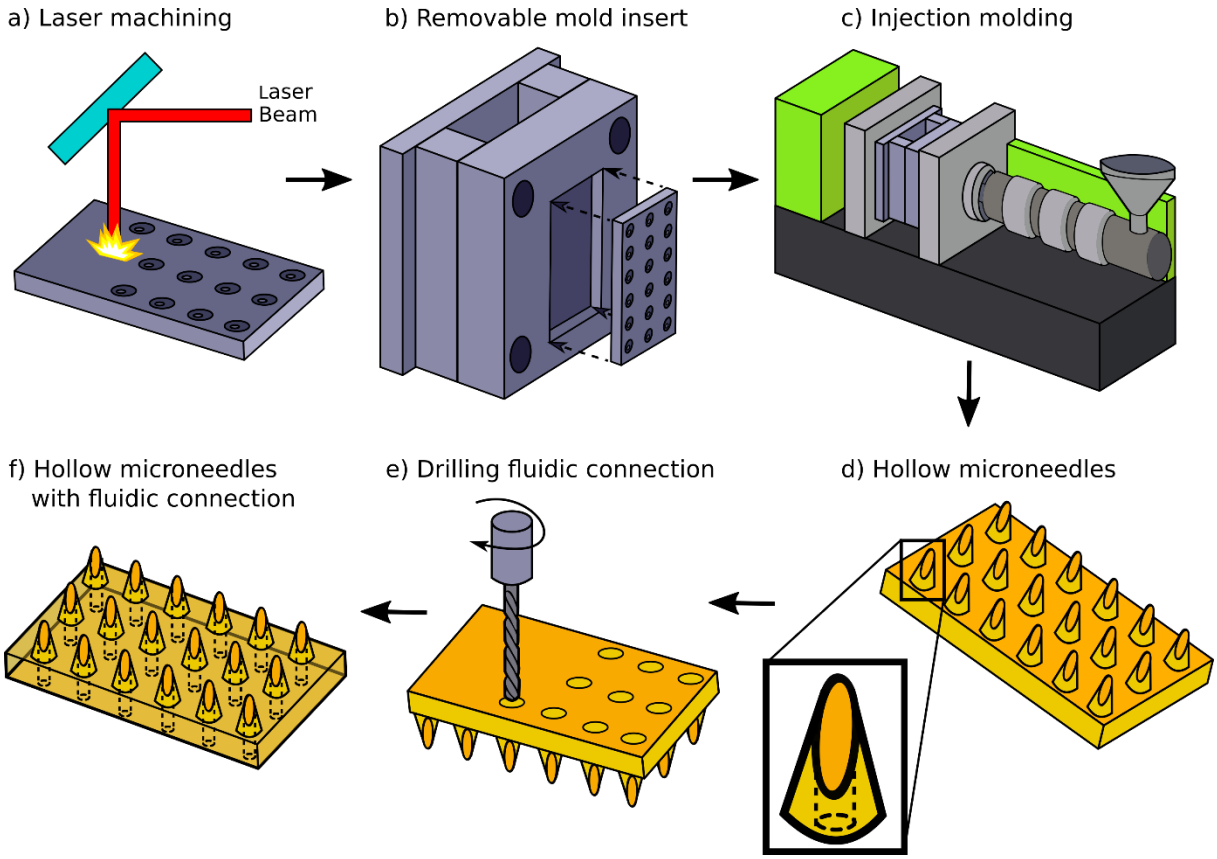
a) Laser machining
Laser
Beam
b) Removable mold insert
c) Injection molding
d) Hollow microneedles
e) Drilling fluidic connection
f) Hollow microneedles
with fluidic connection

Fig. 3

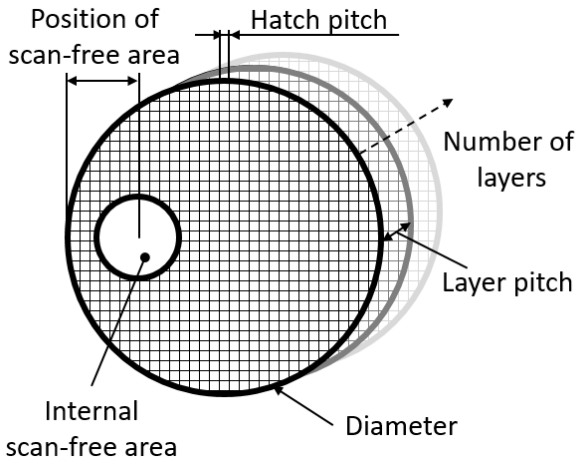
Position of
scan-free area
Hatch pitch
Number of
layers
Layer pitch
Internal
scan-free area
Diameter

Fig. 4

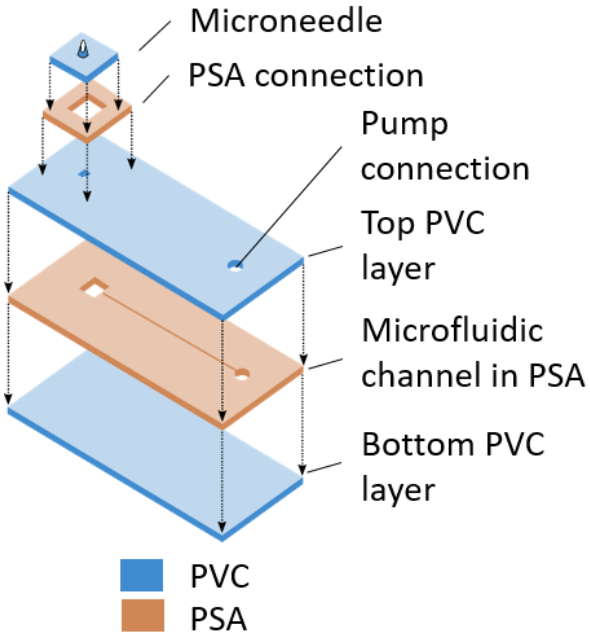
Microneedle
PSA connection
Pump connection
Top PVC layer
Microfluidic channel in PSA
Bottom PVC layer
PVC
PSA

Fig. 5

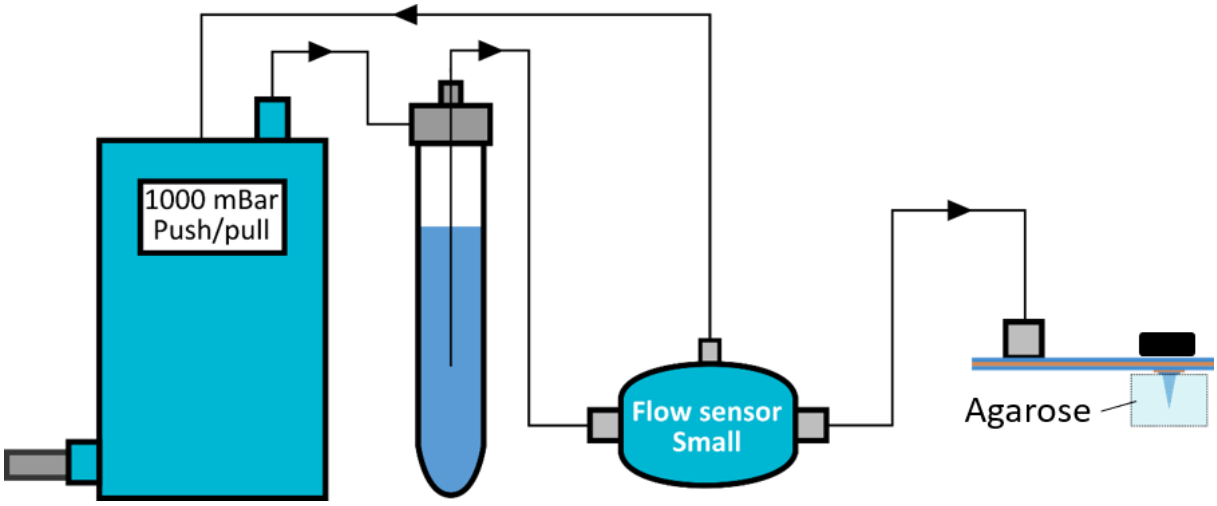

Fig. 6

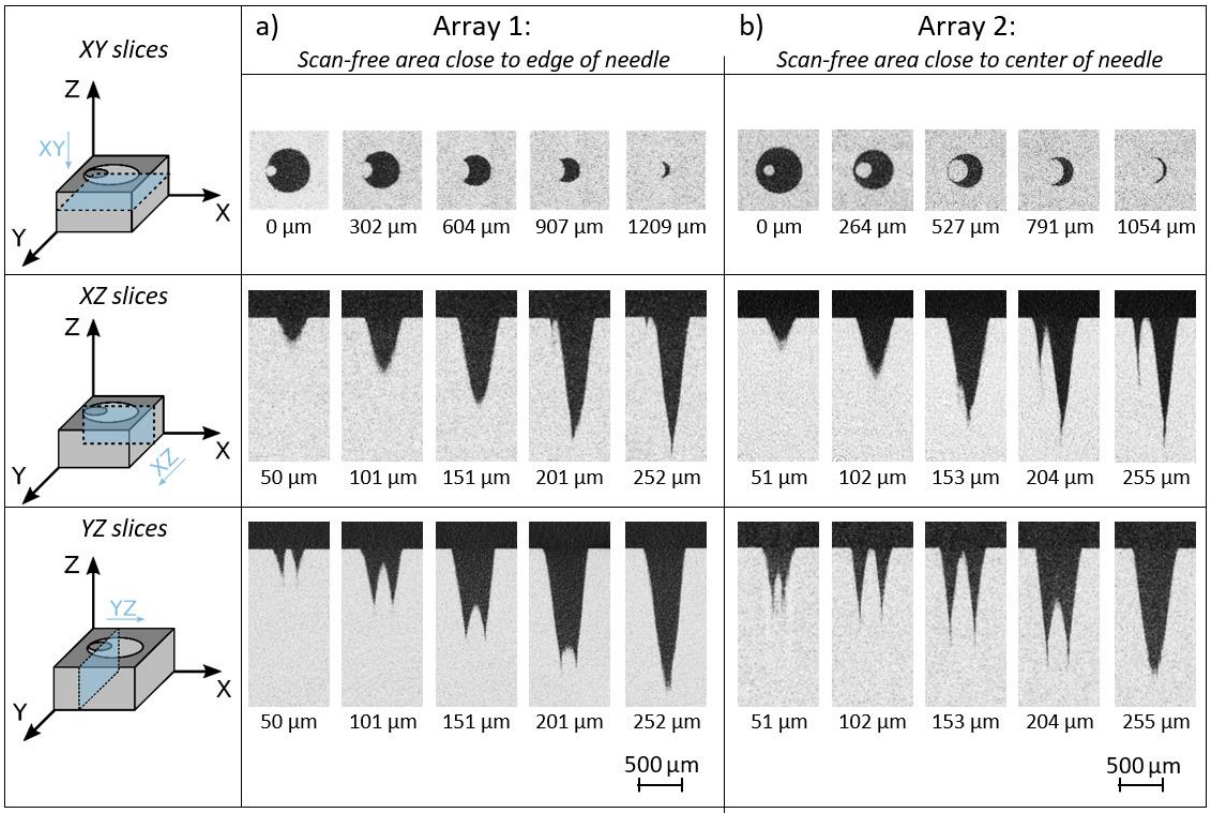
XY slices
Z
XY
X
Y
a) Array 1:
Scan-free area close to edge of needle
b) Array 2:
Scan-free area close to center of needle
0 µm
302 µm
604 µm
907 µm
1209 µm
0 µm
264 µm
527 µm
791 µm
1054 µm
XZ slices
Z
X
Y
XZ
50 µm
101 µm
151 µm
201 µm
252 µm
51 µm
102 µm
153 µm
204 µm
255 µm
YZ slices
Z
YZ
X
Y
50 µm
101 µm
151 µm
201 µm
252 µm
500 µm
51 µm
102 µm
153 µm
204 µm
255 µm
500 µm

Fig. 7

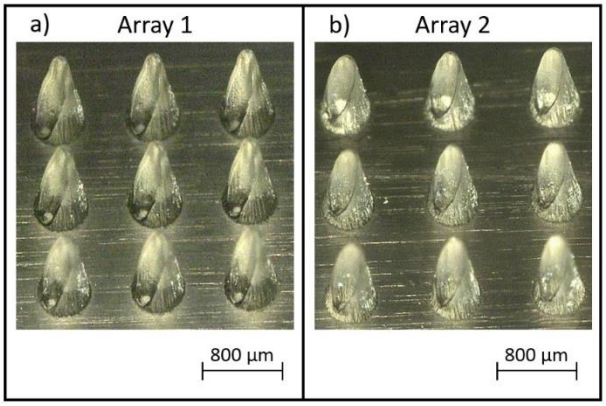

Fig. 8

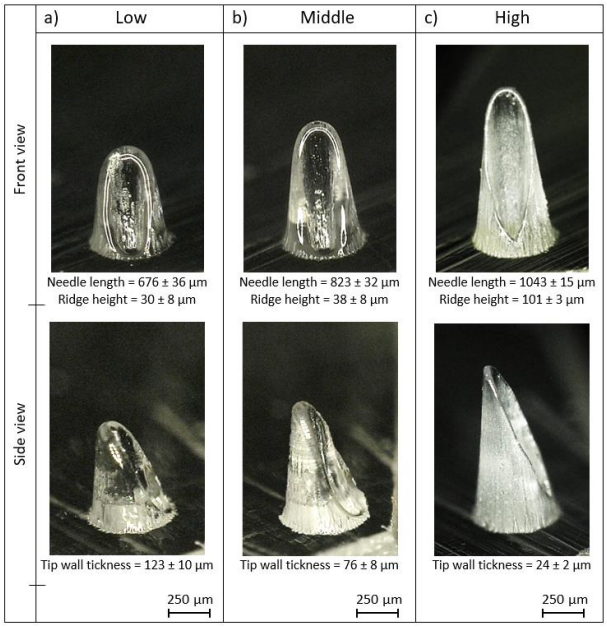
a) Low
b) Middle
c) High
Front view
Side view
Needle length = 676 ± 36 µm
Ridge height = 30 ± 8 µm
Needle length = 823 ± 32 µm
Ridge height = 38 ± 8 µm
Needle length = 1043 ± 15 µm
Ridge height = 101 ± 3 µm
Tip wall tickness = 123 ± 10 µm
Tip wall tickness = 76 ± 8 µm
Tip wall tickness = 24 ± 2 µm
250 µm
250 µm
250 µm

Fig. 9

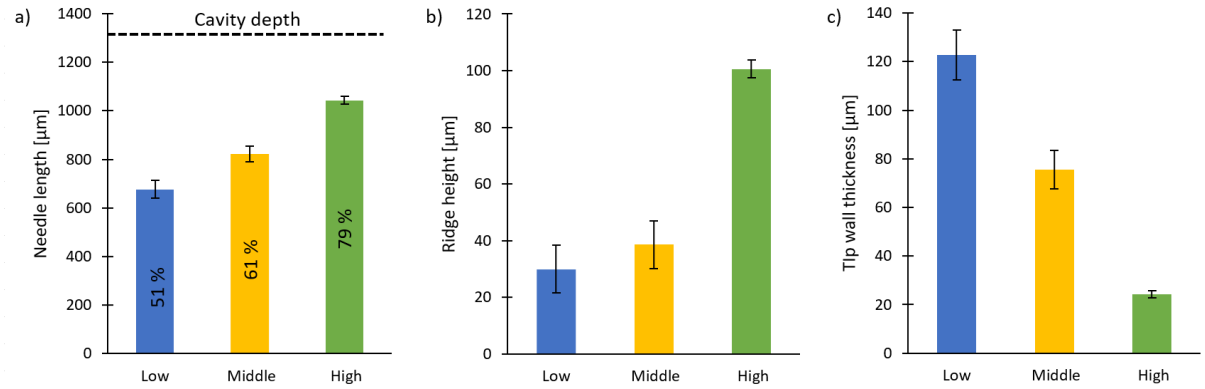
a)
Cavity depth
Needle length [µm]
1400
1200
1000
800
600
400
200
0
51 %
61 %
79 %
Low
Middle
High
b)
Ridge height [µm]
120
100
80
60
40
20
0
Low
Middle
High
c)
Tip wall thickness [µm]
140
120
100
80
60
40
20
0
Low
Middle
High

Fig. 10

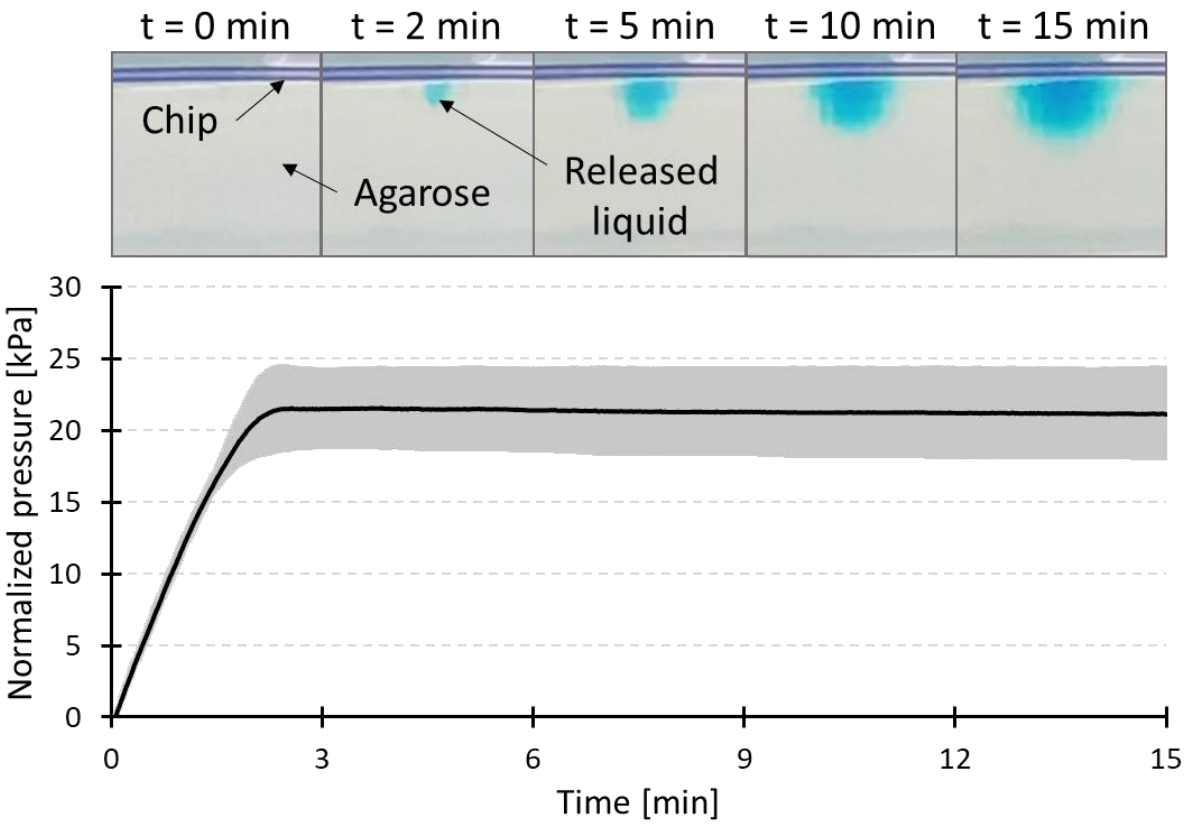
t = 0 min
t = 2 min
t = 5 min
t = 10 min
t = 15 min
Chip
Agarose
Released liquid
Normalized pressure [kPa]
30
25
20
15
10
5
0
0
3
6
9
12
15
Time [min]